



**UNIVERSITY OF LEEDS**

This is a repository copy of *Musculoskeletal Model for Path Generation and Modification of an Ankle Rehabilitation Robot*.

White Rose Research Online URL for this paper:  
<http://eprints.whiterose.ac.uk/161444/>

Version: Accepted Version

---

**Article:**

Jamwal, PK, Hussain, S, Tsoi, YH et al. (1 more author) (2020) Musculoskeletal Model for Path Generation and Modification of an Ankle Rehabilitation Robot. *IEEE Transactions on Human-Machine Systems*. ISSN 2168-2291

<https://doi.org/10.1109/thms.2020.2989688>

---

© 2020 IEEE. Personal use of this material is permitted. Permission from IEEE must be obtained for all other uses, in any current or future media, including reprinting/republishing this material for advertising or promotional purposes, creating new collective works, for resale or redistribution to servers or lists, or reuse of any copyrighted component of this work in other works.

**Reuse**

Items deposited in White Rose Research Online are protected by copyright, with all rights reserved unless indicated otherwise. They may be downloaded and/or printed for private study, or other acts as permitted by national copyright laws. The publisher or other rights holders may allow further reproduction and re-use of the full text version. This is indicated by the licence information on the White Rose Research Online record for the item.

**Takedown**

If you consider content in White Rose Research Online to be in breach of UK law, please notify us by emailing [eprints@whiterose.ac.uk](mailto:eprints@whiterose.ac.uk) including the URL of the record and the reason for the withdrawal request.



[eprints@whiterose.ac.uk](mailto:eprints@whiterose.ac.uk)  
<https://eprints.whiterose.ac.uk/>

# Musculoskeletal Model for Path Generation and Modification of an Ankle Rehabilitation Robot

Prashant K. Jamwal, Member, IEEE, Shahid Hussain, Yun H. Tsoi, and Sheng Q. Xie, Senior Member, IEEE

**Abstract**—While newer designs and control approaches are being proposed for rehabilitation robots, vital information from the human musculoskeletal system should also be considered. Incorporating knowledge about joint biomechanics during the development of robot controllers can enhance the safety and performance of robot-aided treatments. In the present work, the optimal path or trajectories of a parallel ankle rehabilitation robot were generated by minimizing joint reaction moments and the tension along ligaments and muscle-tendon units. The simulations showed that using optimized robot paths, user efforts could be reduced to 80%, thereby ensuring less strain on weaker or stiffer ligaments, etc. Additionally, to limit the moments applied by the robot in stiff or constrained directions, the intended robot path was modified to move the commanded position in the direction opposite to that of the position error. Such online modification of the robot path can lead to a reduction in forces applied by a robot to the subject. Simulation results and experimental findings with healthy subjects using an ankle rehabilitation robot prototype and subsequent statistical analysis further validated that path modification based on ankle joint biomechanics results in a reduction in undesired forces experienced by human users during treatment.

**Index Terms**— ankle joint musculoskeletal modeling, optimization of muscle forces, parallel ankle rehabilitation robot, robot path generation and modification

## I. INTRODUCTION

PHYSICAL orthopedic rehabilitation is one of the most appropriate applications of robots, and this fact is quite apparent from the recent literature on rehabilitation robots and related research. The use of robots has been found to be effective in physical therapy by previous researchers [1-5]. Rehabilitation robots can be used to help therapists in their labor intensive, repetitive work to motivate the patient through interactive user interfaces to exert more effort without getting tired or bored and to improve the rehabilitation process by making it more objective and accurate [6-9]. However, since these robots work in close proximity to the human user, it is important that their interactions and operations are safe, gentle and intuitive [10-12]. Researchers have now started to realize that it is vital to study the human system, specifically the structure and functioning of the musculoskeletal system, while working on the design, actuation and control of a rehabilitation robot [13-16]. The musculoskeletal features of the limbs and joints that are being treated need to be included during the design and control stages for rehabilitation robots [13, 17, 18]. Earlier, while designing a robust impedance controller for an upper limb rehabilitation robot with a single degree of freedom

(DOF), Buerger and Hogan considered human arm impedance as a major design criterion [19]. For a similar robotic application, Miyaguchi et al. [20] used a skeletal model of the human arm to design an impedance controller, and the impedance parameters of the controller were tuned to minimize the extension of certain ligaments.

In a few other instances of rehabilitation robots, researchers have incorporated human-robot interactive moment information in controlling the position error of the robot [11, 21]. Reference trajectory or reference path generation is an important research area in robotics [22, 23]. The reference path for rehabilitation robots is normally predefined by extracting information from biomechanics lab experiments and observations of usual limb paths during activities of daily living (ADL) [11, 24-26]. During robot-assisted rehabilitation, this path is altered using compliance or impedance control strategies that are developed using interaction forces and position errors [17, 24, 27]. Robot path generation from the recordings of subject-specific and trainer-induced leg trajectories is proposed in [28, 29]. On the other hand, the further advanced path generation strategy proposed by Vallery et al. [30] exploits the learning of healthy limb movements in deciding the commanded robot path for hemiplegic patients. Recently, Sartori et al. proposed a hybrid EMG-informed neuro musculoskeletal model [31]. Nevertheless, further work on the validation of this hybrid model is required since presently, it has been validated only in calibration trials. Challenges associated with EMG data acquisition and conditioning, such as cross-talk, electrical and ambient noises, etc. still remain to be addressed. Hong et al. proposed Gaussian process-based trajectory learning to identify individual musculoskeletal parameters from gait motions at different speeds in healthy subjects [32]. This model considers individual subjects' physiological characteristics, such as height, weight, and age, to generate the rehabilitation path. However, the model fails to modify the path in real time based on an individual patient's injury and reduced capabilities. Other works related to the use of biosensors in musculoskeletal modeling [33-35] are worth mentioning here for the entirety of the discussion. However, the use of biosensors and their data acquisition have many challenges, which further adds to the complexity of musculoskeletal modeling [36].

While there have been few previous attempts to take into account interaction forces in the generation and control of the robot path [37, 38], musculoskeletal models have not yet been used in rehabilitation robot online path adaptation. In particular, to the best of our knowledge, no previous research is available wherein an ankle joint musculoskeletal model is used in the

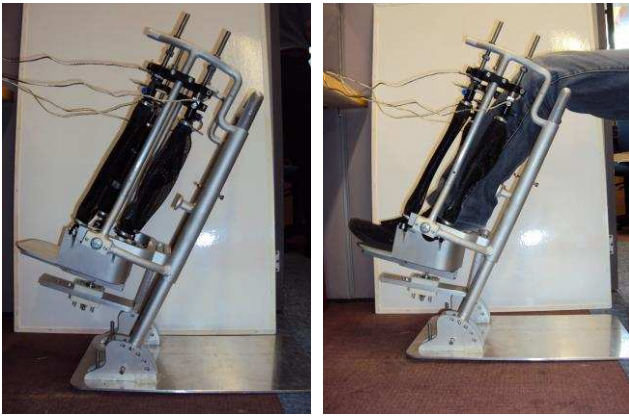


Fig. 1. The parallel ankle rehabilitation robot employed for the experiments.

path planning and adaptation of rehabilitation robots. In their recent work [39], some authors proposed a musculoskeletal model of the ankle joint wherein a thorough investigation of the ankle joint and its articulating musculoskeletal elements was carried out. Apart from the information on joint positions and displacements, the proposed musculoskeletal model is able to provide values of the tensions experienced by ligaments, muscles and tendons and the joint torques resulting from certain motions. Such information can be of relevance, especially in deciding the range of motion treatments prescribed for various musculoskeletal injuries, including ankle sprains. In the initial stage of rehabilitation, the affected joint is subjected to displacements within the range of pain-free motion [40]. Therefore, it is preferred to keep low forces on certain musculoskeletal elements that are in the process of recovery from injuries. A musculoskeletal model is also required to obtain information about the forces generated by injured musculoskeletal elements to decide on the suitability of a given rehabilitation path or suggest an alternative path.

In the present research, optimal rehabilitation trajectories for an ankle rehabilitation robot [41] were obtained. An optimal trajectory is one that requires minimum tensions in the force elements in addition to minimum joint reaction moments. The ankle robot used herein (Fig. 1) is a parallel robot with two platforms, namely, fixed and moving platforms connected together with four linear flexible actuators. These actuators are operated and controlled simultaneously to obtain the position of the moving platform necessary to accommodate the foot-ankle combination of the patients.

In other words, this study investigates the path generation and adaptation of the parallel ankle rehabilitation robot based on a musculoskeletal model of the human ankle joint. The procedure for path generation is represented by an optimization problem whereby a cost function comprising the tensions in ligaments, tendons, and joint reaction moments is minimized. Later, the robot path is modified using the large position errors as kinematic constraints, thereby allowing deviation away from the commanded paths. To the best of the authors' knowledge, reference path generation in real time for rehabilitation robots using a musculoskeletal model has not yet been proposed in the literature. Section II of this paper discusses the methods used for the development of a musculoskeletal model of the human

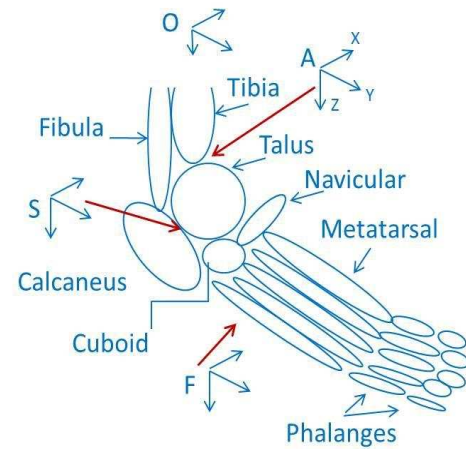


Fig. 2. Pictorial representation of the ankle joint consisting of ankle (A), subtalar (S) and foot (F) coordinate frames

ankle joint and the generation of a rehabilitation path. Section III presents the simulations and results of the reference path modification and its experimental validation using the ankle robot. Section IV provides discussions and conclusions drawn from the present research.

## II. Methods

### A. Musculoskeletal Modeling of the Ankle joint

Musculoskeletal models describing the foot-ankle system have previously been proposed with varying degrees of complexities. Initial models were based on the assumption that the human ankle could be considered a rigid body working like a ball and socket joint [42, 43]. Several advanced models using finite element analysis have also been proposed; however, these models cannot be used in real time owing to their longer run times [44-46]. To model the activation dynamics of human muscles around the ankle joint, most researchers have used the popular Hill-based model [47-50]. However, in modeling the characteristics of ligaments, there is no acceptable unique approach, and while some researchers have modeled ligament behavior as a passive moment of displacement at the ankle joint [43], other studies explicitly modeled ligaments as the tension between spring elements [42, 46]. In light of the above studies, it can be concluded that to estimate tensions applied to ligaments and muscle-tendon units for the path generation problem, their functional models must be obtained. In their previous research [39, 51], authors have carried out detailed modeling of the musculoskeletal elements around the ankle joint. In their previous work, a rigid body-based model was preferred over finite element models to save on computational costs while using the model in real time for robot path generation. In the following subsections, a musculoskeletal model of the ankle joint is briefly described.

#### 1) Kinematics of the Ankle-Foot Joint

Anatomically, the ankle joint lies at the terminal ends of the lower leg bones, i.e., the fibula and tibia, and connects with the foot tarsal bones (mainly with the talus), which is a cluster of seven articulating bones. The three bones jointly form a tight synovial hinge joint that facilitates plantar flexion and

dorsiflexion of the foot. These bones further combine to form two joints, specifically, the ankle and the equally important subtalar joint (Fig. 2). Various ankle motions are realized by the combined subtalar and ankle joint; therefore, the foot-ankle joint can also be called a biaxial joint. The kinematics of such a biaxial ankle joint can be easily defined with respect to a certain fixed orientation using homogeneous transformation matrices that are normally used to describe the orientation and position of rigid bodies. Using transformation matrices for frames relative to each other, it is possible to define a point in another frame without losing its characteristics.

At the onset, the system of homogeneous transformation matrices was defined (as shown in Fig. 2) considering three coordinate frames, namely, the ankle frame (A), the subtalar frame (S) and the foot frame (F). These frames are defined with respect to a stationary global frame (this fixed frame is situated inside the tibia bone and represented as O). For the present research, all the bones right of the phalanges to the cuboid bone and calcaneus are assumed to be a single body, and the translations and orientations of this body are represented by the foot frame (F). The position of the subtalar frame (S), which is located between the talus and calcaneus bones, remains fixed with respect to the global frame, while it is free to rotate about the y-axis in the subtalar frame (S) to realize internal and external rotations. Finally, the ankle frame (A), situated between the tibia, fibula and talus bones, allows flexion motion about the ankle joint axis or about the x-axis of the ankle frame (A). Next, using (1), the position and orientation of the foot frame (F) with respect to the global frame (O) can be obtained with the help of transformation functions of other coordinate frames.

$$T_F^O = T_A^O T_S^A T_F^S \quad (1)$$

## 2) Viscoelastic Behavior of Ligaments:

Ankle ligaments are the soft tissues that connect together the articulating bones at the ankle joint and are referred to as medial and lateral ligaments. A linear viscoelastic model is used here to model the force response of ligaments to a step strain input. The present study uses a combination of springs and dampers in the construction of a viscoelastic model.

We can model the elastic behavior through a simple spring (k), while the viscoelastic behavior can be modeled by a serial arrangement of springs and dashpots. Following Maxwell's model [52], the ligaments can be represented using a parallel combination of a spring-damper unit and another spring element. Ligament forces also have two components (as per Funk's model) [53]: a steady state force component and a time varying component. Here, a spring element is used to quantify strain, whereas the spring damper unit represents the time varying component of the ligament tension.

The elastic response of ligaments predominantly varies linearly with applied strain and can be modeled as in (2) below:

$$F_e(x_0) = G_i(t) A_1 (e^{\frac{x_0}{L_0}} - 1) \quad (2)$$

Here,  $x_0$  is the instantaneous ligament stretch, and  $L_0$  is the ligament's relaxed length. Following Funk's model, the instantaneous force, obtained using (2), is later multiplied by the reduced relaxation function coefficient  $G(t)$  [53].

## 3) Modeling Muscle-Tendon Units:

Muscles connecting bones through tendons have been

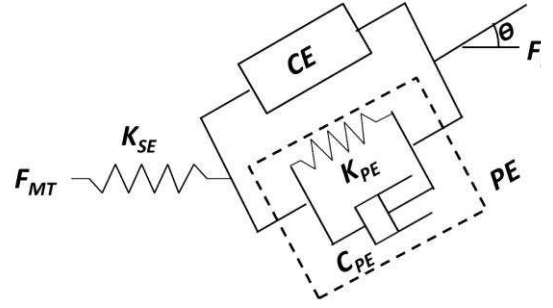


Fig. 3. Muscle-tendon unit modeled with viscoelastic elements.

modeled using the popular Hill-based model [47-50]. Here, the entire muscle-tendon unit is considered, and while tendons are represented as nonlinear springs ( $K_{SE}$ ), the muscles are modeled for their active and passive components. The active part is represented by a contractile element CE, whereas the passive part (connected in parallel to CE) PE determines the passive behavior of the muscle (Fig. 3). The passive behavior of muscle can be modeled using a nonlinear spring ( $K_{PE}$ ) and a damper ( $C_{PE}$ ). A pennation angle  $\theta$  is assumed to be the angle between the directions of the muscle-tendon unit and the applied force.

Contractile element force ( $F_{CE}$ ) is a function of strain ( $\epsilon$ ) and strain rate ( $\dot{\epsilon}$ ) and is normally represented by (3), where  $f_l = -k\epsilon$  and  $f_v = -c\dot{\epsilon}$ . Here,  $A$  represents an activation function of muscles ( $0 < A < 1$ ) and measures the size of the muscle force realized.  $F_{max}$  is the maximum force exerted by the muscle.

$$F_{CE}(A, \epsilon, \dot{\epsilon}) = (AF_{max})f_l(\epsilon)f_v(\dot{\epsilon}) \quad (3)$$

Furthermore, OpenSim software [54, 55] was used to extract information regarding the tendon's force-strain relationships and the parallel element functions. OpenSim can determine subject-specific musculoskeletal model parameters using user-specific inputs and experimental data. Here,  $f_l$  and  $f_v$  are generated based on several data points and cubic spline interpolation. The force-velocity relation is formulated as (4), where  $a_f$  is a factor that depends on the composition of slow and fast twitch fibers in the muscle. The normalized strain rate ( $\dot{\epsilon}$ ) in the contractile element is also considered when calculating the maximum muscle force (3). Material constant parameters  $\alpha$  and  $\beta$  define the force-velocity relationship in the presence of positive muscle stretch velocities. These parameters enable the achievement of the desired limiting value for  $f_v(v_{CE})$  under the condition of muscle velocity approaching infinity or attaining very high values. The strain rate after normalization  $\dot{\epsilon}$  can be written as  $\frac{v_{CE}}{|v_{max}|}$ , where  $v_{max}$  denotes the maximum speed of muscle contraction under consideration.

Subsequently, the dynamics of the muscle-tendon unit are modeled using a state space approach. In this state space model, the length of the CE is considered a state variable. Here, readers are referred to the author's previous work [39] for further details regarding the dynamics of muscle-tendon units. Once the forces and moments applied by ligament and muscle-tendon units at the ankle joints are obtained, the dynamics of the foot and talus can be readily derived.

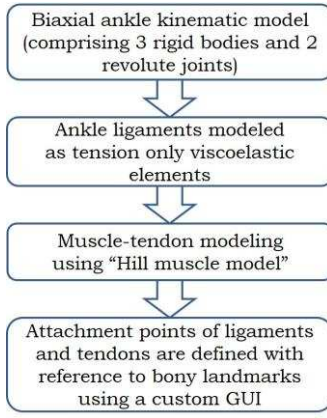


Fig. 4. Development of the musculoskeletal model of the ankle joint

$$f_v(v_{CE}) = \begin{cases} \frac{a_f(1+\dot{\epsilon})}{(a_f-\dot{\epsilon})} & \text{during isotonic contraction} \\ \frac{1+\alpha\dot{\epsilon}}{1+\beta\dot{\epsilon}} & \text{during extension} \end{cases} \quad (4)$$

In the present work, the Newton-Euler approach is used to formulate dynamic equations. Using these formulations, one can convert the task space accelerations to joint space and vice versa based on the kinematic constraints of the ankle model (1). Subsequently, the state space model is developed to describe the overall dynamics of the ankle-foot structure.

It can be argued that such a musculoskeletal model can provide forces along ligaments and tendons in addition to reaction forces and moments at various joints around the ankle under given loading conditions. Finally, this model can be applied for simulations to assess the consequences of various robot paths for the musculoskeletal system.

A graphical user interface (GUI) [51] was also developed during this work to convert the visual information into quantitative data. A 3D surface model for the ankle joint was constructed for the GUI in MATLAB® [56]. The bone surface geometry was utilized to define the force element attachment points. Various steps performed during the development of the abovementioned musculoskeletal model of the ankle joint are further explained using a block diagram (Fig. 4).

## B. Rehabilitation Path Generation

Desired or reference paths for rehabilitation robots are normally well-defined paths that are encountered during ADLs. During therapeutic treatments, these motion paths require altering after acquiring more information about the patient's abilities from their interaction with robots and subsequent measurements [29]. This information can also be obtained from the movements of healthy limbs in hemiplegic patients [30]. However, musculoskeletal system modeling remains the key for such measurements or observations to generate rehabilitation paths, especially in ankle joint rehabilitation.

Ankle joint biomechanics can also be applied to examine how various motion paths affect tensions in force elements such as ligaments and muscle-tendon units. Thus, apart from generating robot paths, musculoskeletal models can also help in the evaluation of rehabilitation paths. Normally, excessive tensioning of ligaments causes ankle sprains; thus, to avoid

further injuries, forces along weaker ligaments are required to remain small. The reaction moment at the ankle joint is another important variable to be considered when deciding the robot path. In fact, the ankle joint is not a rigid revolute joint since the constituent bones, namely, the tibia and fibula, are connected via ligaments and can shift slightly upon application of large moments in the direction perpendicular to the joint axis, leading to dislocation.

From the above discussion, it is evident that a rehabilitation path can only be decided after assessing the tensions in the force element and the joint reaction moments. Here, the optimization problem formulation for a cost function incorporating these two variables is discussed in brief for completeness and continuity.

## Optimization Problem Formulation

The rehabilitation path, characterized by several key points, can be drawn using cubic splines. Cubic splines, that represent the position changes of the ankle and subtalar joint, are denoted by an independent variable  $\lambda$ . In equation (7),  $f_{ij}(\lambda)$  are cubic functions representing the ankle or subtalar joint displacements with respect to  $\lambda$ , and  $i = a, s$  denotes the ankle-subtalar joint path, whereas  $j = 1, \dots, N$  denotes the index for the cubic spline segments required to complete the path. Furthermore,  $c_{ijk}$  denotes a scalar coefficient (constant) of the  $k^{\text{th}}$  exponent in the cubic functions.

$$\theta_a = f_a(\lambda) \quad (5)$$

$$\theta_s = f_s(\lambda) \quad (6)$$

$$f_{ij}(\lambda) = c_{ij0} + c_{ij1}\lambda^N \quad (7)$$

Where:

$$f_{ij}(\lambda_{j-1}) = p_{i,j-1} \text{ and } f_{ij}(\lambda_j) = p_{i,j}$$

In the above formulations (5-7),  $p_{ij}$  denote the key points (as mentioned above) of the ankle and subtalar joint paths. Given the normalized and cumulative Euclidean distance between successive key points on the  $\theta_a$ - $\theta_s$  plane, the independent variables  $\lambda_j$  are computed automatically. The independent variable  $\lambda_0$  is always zero, and  $\lambda_N$  remains unity, given that normalization is accomplished with regard to the total Euclidean distance.

Next, a cost function can be defined in terms of tension in the force elements and the joint reaction forces (which are required to be minimized), as in (8). Here,  $t_{fe}$  denotes a vector of force elements for a given set of joint displacements at the steady state. On the other hand,  $\mu_{AS}$  depicts the vector of reaction moments at the ankle and the subtalar joint. The Euclidean distance along the commanded path is given by  $\gamma$ . The steady state tensions are calculated while ignoring the dynamics of force elements. Next, we determine the reaction moments in two steps. In the first step, we identify the minimal norm external wrench, which is needed to keep the dynamic model of the ankle-foot in steady state. In the second step, we determine the reaction moment vector by replacing the resultant wrench in the moment equations.

$$C = \int [t_{fe}^T \quad \mu_{AS}^T] W \begin{bmatrix} t_{fe} \\ \mu_{AS} \end{bmatrix} d\gamma \quad (8)$$

Since  $\gamma$  and  $\lambda$  are related as given in (9), the cost function is rewritten as in (10).

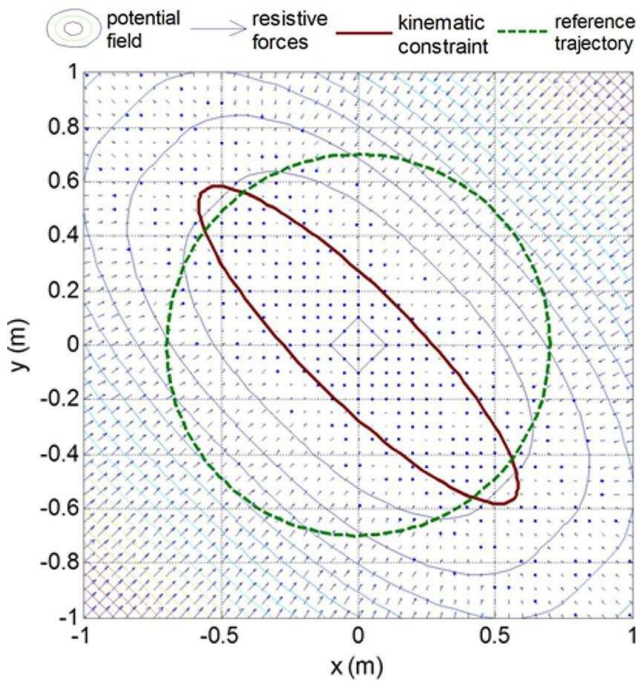


Fig. 5. The environment used in the simulations during the case study represented graphically.

$$\frac{dy}{d\lambda} = \sqrt{\left(\frac{d\theta_a}{d\lambda}\right)^2 + \left(\frac{d\theta_s}{d\lambda}\right)^2} = \sqrt{\left(\frac{df_a(\lambda)}{d\lambda}\right)^2 + \left(\frac{df_s(\lambda)}{d\lambda}\right)^2} \quad (9)$$

$$C = \int [t_{fe}^T \quad \mu_{AS}^T] W \begin{bmatrix} t_{fe} \\ \mu_{AS} \end{bmatrix} \sqrt{\left(\frac{df_a(\lambda)}{d\lambda}\right)^2 + \left(\frac{df_s(\lambda)}{d\lambda}\right)^2} d\lambda \quad (10)$$

Owing to the optimization and subsequent reduction in the cost function, a significant decrease in the joint reaction moments in addition to the ligament tensions is expected.

### C. Reference Path Modification

Apart from generating robot paths that require lower joint reaction moments and ligament tensions, rehabilitation robot paths also need to be modified during treatments. To offer safe treatment, applied forces should be reduced when increased muscle stiffness or other constraints are encountered, and as a consequence, there will be a noticeable change in the reference path. In other words, the reference path needs to be modified to change the desired position or shift in the direction opposite to the position error. However, to avoid frequent changes in the paths and resulting perturbations, a threshold error (below which the path remains unchanged) may be considered that affects such path modification rules. As a result of such modification, the desired path will be followed as long as the stiffness or resistive force applied by the subject is small. Furthermore, a modification of the reference path will be allowed when the desired position is placed in a stiff or constrained zone of the robot workspace, resulting in a large position error.

The path modification rule proposed in this research is formulated as (11), where  $x'_d$  is the changed or modified path,  $x_d$  is the reference path, and  $\Delta x_d$  is the correction in the original path obtained using (12). The regression matrix  $Y$  in (12) is determined based on the activation levels ( $\alpha$ ,  $\beta$ ) of a set of Gaussian radial basis functions that are spatially distributed. Furthermore,  $\hat{\rho} \in \mathbb{R}^n$  is the parameter vector of the weights

related to the Gaussian radial basis functions. The modification law for the path correction may also be represented as (13), where ' $x_e$ ' is the position error vector, and ' $x_{e,th}$ ' is the threshold error as reported above. Finally, to obtain the minimal norm solution for the time derivative of parameter ( $\hat{\rho}$ ) in (13), the pseudoinverse (14) is used.

$$x'_d = x_d - \Delta x_d \quad (11)$$

$$\Delta x_d = Y \hat{\rho} \quad (12)$$

$$Y \hat{\rho} = -\alpha Y \hat{\rho} + \beta (Y Y^T)^{-1} \max\left(0, 1 - \frac{x_{e,th}}{\|x_e\|}\right) x_e \quad (13)$$

$$\dot{\hat{\rho}} = -\alpha Y^T (Y Y^T)^{-1} \Delta x_d + \beta Y^T \max\left(0, 1 - \frac{x_{e,th}}{\|x_e\|}\right) x_e \quad (14)$$

### Simulated Case Study for Path Modification

In the face of uncertain kinematic constraints posed by the human user, an adaptation law (13) would undesirably continue to enhance the applied force in the directions of the constraints. This increase in interaction force will try to correct the end effector position irrespective of whether the current position is lagging or leading the desired trajectory. However, during rehabilitation treatments, subjects should be allowed to deviate slightly from the desired trajectory. This issue, in particular, has been addressed by using a potential function to determine the corrective forces applied on the user [57]. Owing to this potential function, the user will not experience resistance when the end effector deviates from the desired rehabilitation trajectory. However, to address this problem, control and adaptation laws are modified during this study, as discussed below. Later, hardware-in-loop simulations are carried out to evaluate the efficacy of the trajectory modification laws. During the simulations, a two-dimensional virtual environment is used, and the stiffness behavior of the environment is determined by superimposing several potential functions. These potential functions were chosen such that there exists a place near the origin of the workspace that has constant potential energy and therefore zero stiffness.

Moreover, the environment was made to be anisotropic with different values for stiffness along different directions. However, constant viscous damping was considered during the simulation experiments.

The robot used during hardware-in-loop simulations is a parallel ankle rehabilitation robot [7] that has four simultaneously actuating limbs (Fig. 1). This robot has a parallel mechanism that can provide the requisite three rotational dofs at the ankle joint from the simultaneous actuation of four linear actuators. The ankle robot has a moving platform that houses the foot-ankle combination and is connected with a fixed frame through four actuators, as explained in the previous section [41].

The potential function directions were also rotated along with the global reference frame of the robot. The environment (human user) is defined using a potential function given by (15), where  $u$  and  $v$  are the coordinate variables of the environment. Furthermore,  $u_{01}$  and  $u_{02}$  are the minimum and maximum limits, respectively, where the potential function is assumed to be constant along the  $u$  direction (similar notations are used for the  $v$  direction). The rotation ( $\Phi$ ), which transforms the global reference frame into the principal reference frame, defines the environment. Since the potential function ( $p_{tot}$ ) depicts energy,

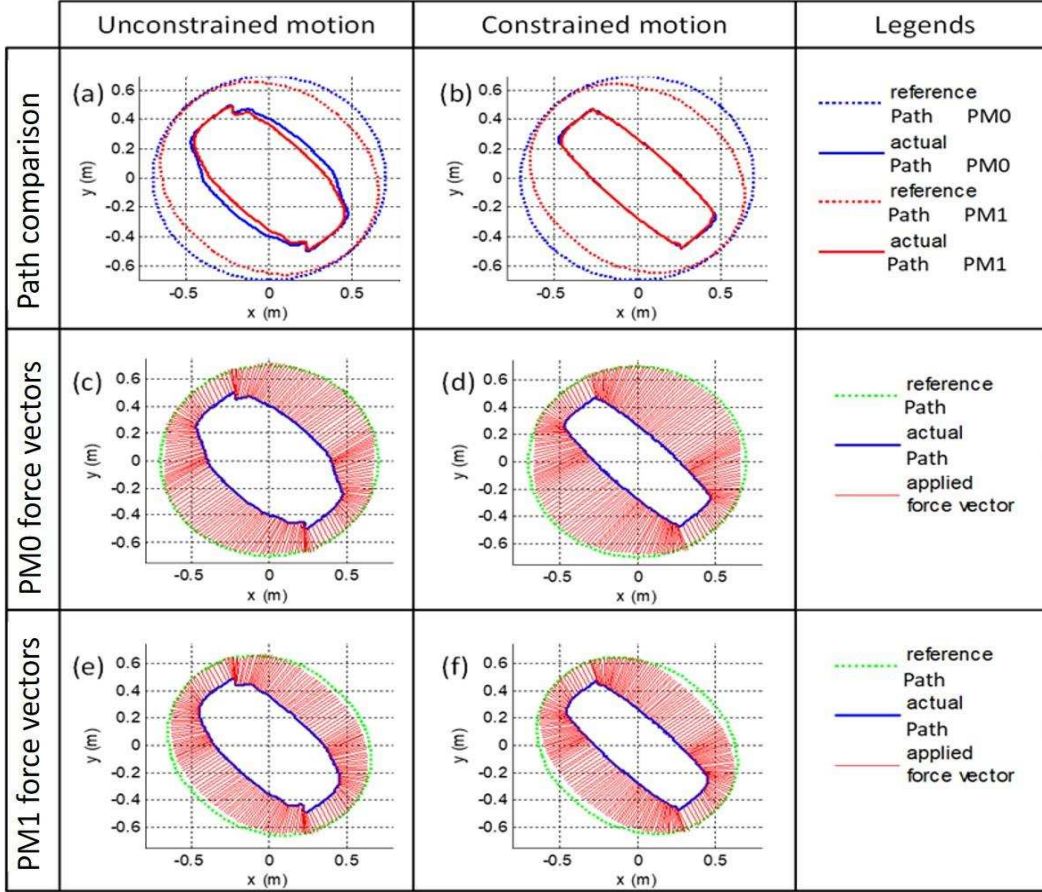


Fig. 6. Trajectory modification module in the simulations: Reference (dotted lines) and actual trajectories (solid lines) are compared for the cases of (a) unconstrained and (b) constrained motions. Force vectors applied with no trajectory modification during (c) unconstrained and (d) constrained motions. Force vectors during trajectory modification during (e) unconstrained and (f) constrained motions. PM1 specifies that the path modification module is activated whereas PM0 indicates that it is not activated.

its partial differentiation provides resistive forces within the environment along the directions of interest.

$$p_{tot} = \sum_i p_i \quad (15)$$

where:

$$\begin{aligned}
 p_1 &= \frac{1}{2}k_1[\min(0, u - u_{01})]^2 \\
 p_2 &= \frac{1}{2}k_2[\max(0, u - u_{02})]^2 \\
 p_3 &= \frac{1}{2}k_3[\min(0, v - v_{01})]^2 \\
 p_4 &= \frac{1}{2}k_4[\max(0, v - v_{02})]^2 \\
 \begin{bmatrix} u \\ v \end{bmatrix} &= \begin{bmatrix} \cos \Phi & \sin \Phi \\ -\sin \Phi & \cos \Phi \end{bmatrix} \begin{bmatrix} x \\ y \end{bmatrix}
 \end{aligned}$$

Next, to reduce the forces applied to the environment (i.e., when kinematic constraints are encountered, which vary considerably among users), some changes are proposed for the adaptation law during experimental simulations. The kinematic constraints were introduced in the form of an ellipse that is positioned and rotated about the global reference frame of the ankle robot. Constraints introduced in this manner can be explained mathematically by (16), while  $l_a$  and  $l_b$  represent the minor and major axes, respectively, and the angle between the semi-minor axis and the  $x$ -axis is given by  $\varphi$ . Here,  $C_\varphi$  and  $S_\varphi$  are abbreviations for the cosine and sine of  $\varphi$ , respectively.

$$\left[ \left( \frac{C_\varphi}{l_a} \right)^2 + \left( \frac{S_\varphi}{l_b} \right)^2 \right] x^2 + 2 \left( \frac{1}{l_a^2} - \frac{1}{l_b^2} \right) C_\varphi S_\varphi xy$$

$$+ \left[ \left( \frac{S_\varphi}{l_a} \right)^2 + \left( \frac{C_\varphi}{l_b} \right)^2 \right] y^2 \leq 1 \quad (16)$$

Whenever the position of the ankle robot shifts outside the constraint boundary, a large stiffness is introduced, signaling that the robot path needs to be modified. To compute the resistive forces at the time when the system violates (16), the point on the ellipse that is nearest to the current position has to be determined. It is important to mention here that the line connecting the current point to this point will be collinear to the normal drawn to the ellipse at this nearest point. Later, by applying the distance between the current and the nearest point and the large stiffness (which is used to penalize motion beyond the constraint boundary), the resistive force was calculated. For motion along the normal direction to the constraint surface, viscous damping was also introduced.

### III. SIMULATIONS, EXPERIMENTS AND RESULTS

Several experimental simulations were carried out considering the environment, as shown in Fig. 5. Here, the potential function is plotted in the form of a contour plot, whereas the resistive force vectors corresponding to the potential function are shown as a quiver plot. The state space model implemented in these simulation experiments uses a point mass traversing within this environment (Fig. 5), while it is assisted by a propulsion force vector through a control law

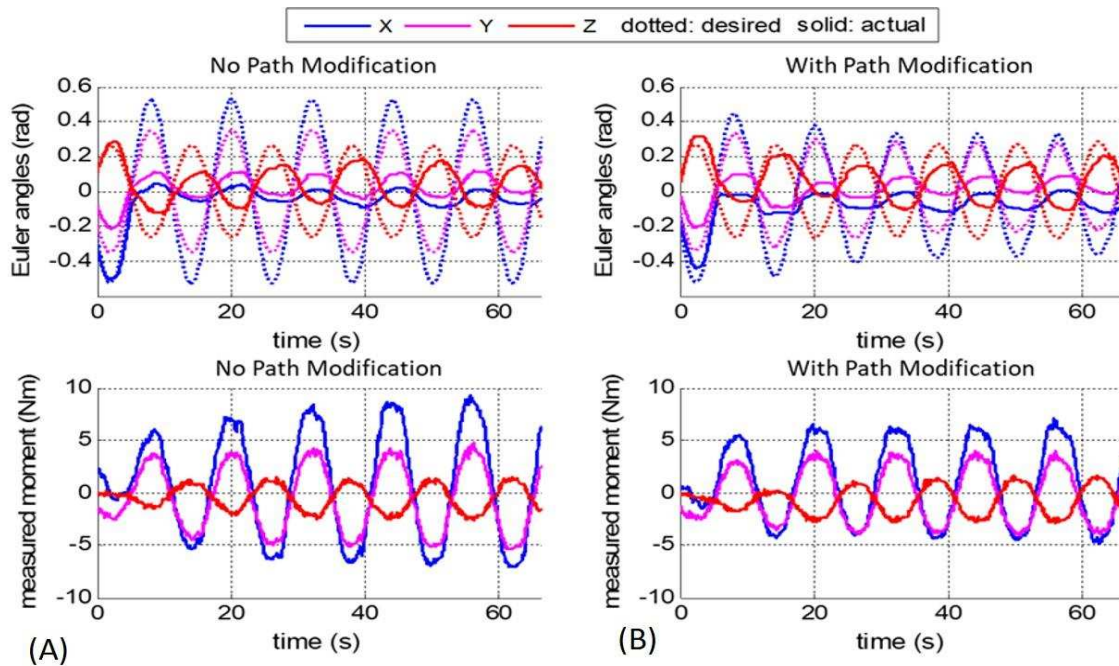


Fig. 7. Reference versus actual foot orientations and estimated interaction moments observed during constrained motion experiments before (A) and after (B) reference path modification. Experimental results averaged over ten subjects are presented.

[4, 58]. The reference path used during experimental simulations is also shown as the green dashed line in Fig. 5.

When starting simulations, the initial position of the robot path is located at the origin. A straight line reference path in the vertical direction guides the reference point to the circular reference path starting from the origin. The period of this path is 6 s, which goes in the clockwise direction on the  $x$ - $y$  plane.

The results from 15 cycles of simulation runs along the reference path were obtained and plotted. The robot was operated under four controlled operating modes: a) the passive and unconstrained mode; b) the passive and constrained mode; c) the active and unconstrained mode; and finally, d) the active and constrained mode. In the passive mode, the robot controller was using a force applied to the passive point mass. In the active mode, an additional force vector was applied to emulate the active participation of the human user. This additional force vector was created by using a force of constant magnitude along the direction of travel of the reference path. An elliptic constraint, as mentioned above, was also applied to simulate the constrained motion. This constraint is represented in Fig. 5 as the brown ellipse.

#### A. Simulated results for the effects of reference path modification

The overall objective of this research was to allow changes in the nominal reference path of the ankle robot so that excessive position errors are minimized. It is important to keep in mind that the force exerted on the environment (human user) is always proportional to this position error and that minimizing this position error will prevent large forces from being exerted to the environment. Simulations were carried out and analyzed under the two operating modes, namely, the passive unconstrained and passive constrained modes. The first row of plots in the simulation results shown in Fig. 6 depicts the

reference path in dotted lines and the actual path in solid lines obtained from the two control approaches: PM0 (blue lines) when the path modification is not considered, and PM1 (red lines) when the path modification is considered and performed. Force vectors produced during these approaches are shown in the second and third rows in the same figure (Fig. 6). Plots illustrated in the left column are the simulation results without considering kinematic constraints in the environment, while the simulation results in the right column were obtained considering kinematic constraints.

It is quite apparent from the results (Fig. 6) that when using the proposed path modification module, the reference paths are shrunk for the constrained as well as for the unconstrained environments. However, even greater reductions can be observed in the stiff and constrained directions. As a result, a close agreement can be observed between the shape of the changed reference path and the actual motion path. However, this has led to less movement in the stiff directions for the unconstrained case. When we considered the forces being applied, it was seen that the levels of the forces observed using path modification were noticeably less than those obtained without path adjustment. It is important to mention here that during these simulations, the feed forward force adaptation law was considered to have a linear dependence on error.

This further suggests that using a path modification routine in the control law can enhance the performance of human-robot interaction throughout constrained and active motions.

#### B. Experimental Validation with an Ankle Robot

An ankle rehabilitation robot that provides three dofs to the ankle joint for its anatomical range of motion (ROM) was developed and used during the present research. As shown in Fig. 1, this robot employs four parallel pneumatic muscle actuators, which in turn provide rotational motion at the end

platform, where the foot of the subject is secured [7]. Experiments were conducted in which healthy subjects used the ankle rehabilitation robot. Ten subjects (10 males; mean age 28.6 years) were asked to participate in these experiments. Experiments with ten subjects provide nine statistical degrees of freedom (df). Appropriate ethics approval was received to run experiments involving healthy subjects.

Subjects were initially asked to become acquainted with the robot and were allowed to move while the attached robot was completely passive. During the experiments in the active mode, sensor data were obtained, averaged and plotted (Fig. 7). Variability in the observations obtained from the ten subjects surrounding the mean are expressed in terms of standard deviations. First, the variances at the normalized data points were obtained from these ten experiments. The averaged standard deviation was later computed from the average of these variances. The averaged standard deviations from all the experiments with the subjects are presented in Table 1 to provide an approximation of the inter-subject variability.

Table 1. Standard deviations of the observations obtained from experiments involving subjects

Euler angles (Radians)	Before PM	After PM	Joint interaction moments (Nm)	Before PM	After PM
X_actual	0.022	0.038	X_Moments	2.35	2.42
Y_actual	0.024	0.031	Y_Moments	3.31	3.04
Z_actual	0.038	0.043	Z_Moments	2.05	2.53

The results presented in Fig. 7 show a substantial decrease in the estimated foot-robot interaction moment as a consequence of the reference path modification. However, to further evaluate and quantify the significance of this intervention, a statistical test was conducted.

Since the data were obtained from experiments with subjects, a distribution-free nonparametric test is an appropriate choice. There are many such tests available; however, since the observation and the outcomes are not independent, tests such as the Mann-Whitney U-test cannot be recommended. Instead, a nonparametric statistical test called the Wilcoxon signed rank test [59] was used to gauge the statistical significance of the difference between means of the two data sets, i.e., those with and without reference path modification. As a result of this test, whether the intervention in the form of reference path modification is significant can be determined.

Data obtained from both experiments (i.e., those with and without path modification) for reference foot orientations, actual foot orientations and interaction moments were tabulated. Later, the Wilcoxon signed rank test was conducted to compare data between the two experiments and establish the significance of reference path modification.

The experimental data for the ankle trajectories and moments (Fig. 7) are cyclic in nature (having both positive and negative values) and therefore require normalization. First, differences ( $\Delta_i$ ) between the row elements ( $i^{th}$ ) of the two columns (e.g., normalized X Euler angles desired with and without path modification) were calculated. The absolute values of these differences ( $\Delta_i$ ) were ranked by giving the lowest rank to the smallest difference and the largest rank to the highest absolute

difference. Zero difference samples were discarded, and those with the same difference were given averaged ranks. The sum of the ranks for positive and negative differences ( $W_i^+$ ,  $W_i^-$ ) was calculated, and the critical z-value for a two-tailed test was recorded (Table 2). The null hypothesis tested here was that the median difference in the data between the two experiments is zero. A simple approach was adopted to test this hypothesis, whereby critical z-values were computed and used to find p-values [59]. While the z-score helps in deciding whether to reject the null hypothesis, the p-value gives the probability for false rejection of the null hypothesis. It is known that a critical z-value for the 95% confidence interval should be 1.96 with a 5% level of significance ( $p = 0.05$ ). In other words, to reject the null hypothesis, the sample z-value should be 1.96 or higher, while the two-sided p-value should be less than 0.05. The results obtained from the Wilcoxon signed rank test are shown in Table 2.

Table 2. Results for the z-values and two-sided p-values from the Wilcoxon signed rank test

	z-value	p-Values
X Euler desired	3.466	0.00053
Y Euler desired	3.046	0.0023
Z Euler desired	2.302	0.0213
X Euler actual	9.146	$5.884e - 20$
Y Euler actual	1.960	0.0499
Z Euler actual	5.439	$5.32e - 8$
X_Moments	2.865	0.0044
Y_Moments	2.81	0.005
Z_Moments	17.904	$1.078e - 21$

From the results shown in Table 2, it is evident that all the z-values are greater than the 1.96 threshold; therefore, the null hypothesis is rejected. This further means that the reference and actual foot orientations, in addition to the interaction moments, changed significantly after applying the path modification. Moreover, the probability for false rejection of the null hypothesis (p-value) was again very low ( $p < 0.05$ ) for all the observations. However, higher z-values for three observations (X\_Euler actual, Z\_Euler actual & Z\_Moments) are a matter of concern and require discussion. A higher z-score ( $> 3.00$ ) indicates that the data values are many standard deviations away from the mean value. In the present case, this further resulted in a shift in the means of the two data sets. For instance, the mean absolute 'X\_actual' Euler angle before and after path modification was found to be 0.0846 rad. and 0.0666 rad., respectively.

The rationale behind the development and use of the path modification module was to adapt the reference path to compensate for position errors and thereby reduce forces experienced by human users during robot-assisted treatments. Subsequent to the experiments and analysis of the results, it was established that the interaction force that exists between the robot and the user can be modified by altering the reference path based on previously learned position errors. In the present research, the excessive position errors are regarded as the presence of kinematic constraints. Accordingly, a robot path modification scheme is devised to decrease the interaction forces in the regions of excessive position errors.

#### IV. DISCUSSION AND CONCLUSION

Analyzing the results from Figs. 6 and 7 and Table 2, it is clear that with activation of the path modification module, a significant reduction in the robot reference trajectory and the interaction moment from the estimated values can be achieved. It can also be noticed that owing to the “shrinking” of the reference path (Fig. 7), position error reduction and ultimately a decreased feed forward moment can be obtained. This further explains that the path modification approach proposed here is successful in decreasing requisite feed forward moments, especially when larger position errors are encountered. It has also been shown statistically that by altering the reference path alone, a significant decrease in force applied by the robot can be achieved. This reduction in forces can even be larger than the reduction in the moment contribution from an impedance controller. It is important to mention here that our approach does not require the use of biosensors, which increases complexity in terms of data acquisition and subsequent signal processing [32-35]. However, there is one shortcoming of path modification that was determined from experimentation using this control module. The problem encountered is the presence of high frequency oscillations in the actuators for large values of parameter  $\beta$  (14). This indicates that there is a limit on how quickly the path can be adapted if the stability of the system is to be maintained. The research work proposed in this manuscript can be summarized as follows.

First, a musculoskeletal model for the ankle joint was developed and presented in this research to obtain tensions in different force elements, such as ligaments and muscle-tendon units. Evidently, this model can also provide us with the joint reaction moments. Second, application of this model in the rehabilitation path generation routine suggested that the ideal path between two foot configurations is not necessarily the one with the minimal path length. Rather, the path that requires minimum tensions in the force elements around the joint should be preferred, especially when the robots are being operated in close proximity to human users, such as in the present case of ankle rehabilitation. Furthermore, using simulations and experiments on a prototype ankle rehabilitation robot with healthy subjects, it was observed that when using robot path modification, a noticeable reduction in the applied robot actuator forces can be achieved. The intervention, in the form of robot path modification, was also tested statistically for its significance. A nonparametric test called the Wilcoxon signed rank test was conducted [59], and it was found that the observations after the intervention were significantly changed. The experiments and results (pertaining to the reduction in interaction moments) presented in this paper, therefore, support the hypothesis that a musculoskeletal ankle model can be applied to improve the initial path for better performance and safety. To the best of our knowledge, reference path generation for rehabilitation robots based on musculoskeletal models has not been extensively performed previously.

Nonetheless, the musculoskeletal model used during this research was constructed based on standard information about musculoskeletal components. However, the surface geometry of the foot bones was obtained from a random CT scan, which was not related to the subject who took part in the experimental trials. Owing to the nonsubject specific nature of the ankle

model, it cannot be expected to be flawless. While the “generic” ankle musculoskeletal model is able to provide sufficient information on the ankle joint behavior required to test our proposed path planning and modification scheme quantitatively, the development of a subject-specific model will be carried out in the future, which will be important in the generation of a rehabilitation path with more accurate prediction of tensions along the force elements.

#### REFERENCES

- Hussain, S., State-of-the-Art Robotic Gait Rehabilitation Orthoses: Design and Control Aspects. *NeuroRehabilitation*, 2014 DOI: 10.3233/NRE-141174.
- Jamwal, P.K., S. Hussain, and S.Q. Xie, Review on design and control aspects of ankle rehabilitation robots. *Disability and Rehabilitation: Assistive Technology*, 2015. **10**: p. 93-101.
- Reinkensmeyer, D.J., J.L. Emken, and S.C. Cramer, Robotics, motor learning, and neurologic recovery. *Annual Review of Biomedical Engineering*, 2004. **6**: p. 497-525.
- Jamwal, P.K., et al., Impedance Control of an Intrinsically Compliant Parallel Ankle Rehabilitation Robot. *IEEE Transactions on Industrial Electronics*, 2016 (In press). DOI: 10.1109/TIE.2016.2521600.
- Lu, R., et al., Development and learning control of a human limb with a rehabilitation exoskeleton. *IEEE Transactions on Industrial Electronics*, 2014. **61**(7): p. 3776-3785.
- Hussain, S., et al., An intrinsically compliant robotic orthosis for treadmill training. *Medical Engineering and Physics*, 2012.
- Jamwal, P.K., et al., An adaptive wearable parallel robot for the treatment of ankle injuries. *IEEE/ASME Transactions on Mechatronics*, 2014. **19**(1): p. 64-75.
- Roy, A., et al., Robot-aided neurorehabilitation: A novel robot for ankle rehabilitation. *IEEE Transactions on Robotics*, 2009. **25**(3): p. 569-582.
- Saglia, J.A., et al. Control strategies for ankle rehabilitation using a high performance ankle exerciser. in *Proceedings - IEEE International Conference on Robotics and Automation*. 2013.
- Hussain, S., S.Q. Xie, and P.K. Jamwal, Robust Nonlinear Control of an Intrinsically Compliant Robotic Gait Training Orthosis *IEEE Transactions on Systems, Man, and Cybernetics—Part A: Systems and Humans*, 2013 **43**(3): p. 655-665.
- Hussain, S., S.Q. Xie, and P.K. Jamwal, Adaptive Impedance Control of a Robotic Orthosis for Gait Rehabilitation. *IEEE Transactions on Cybernetics*, 2013 **43**(3): p. 1025-1034.
- Hussain, S., S.Q. Xie, and P.K. Jamwal, Control of a Robotic Orthosis for Gait Rehabilitation. *Robotics and Autonomous Systems*, 2013. **61**: p. 911-919.
- Hussain, S., S.Q. Xie, and P.K. Jamwal, Effect of Cadence Regulation on Muscle Activation Patterns during Robot Assisted Gait: A Dynamic Simulation Study. *IEEE Journal of Biomedical and Health Informatics* 2013 **17**(2): p. 442-451.
- Shelburne, K.B., M.R. Torry, and M.G. Pandy, Contributions of muscles, ligaments, and the ground-reaction force to tibiofemoral joint loading during normal gait. *Journal of Orthopaedic Research*, 2006. **24**(10): p. 1983-1990.
- Knaepen, K., et al., Human-robot interaction: Kinematics and muscle activity inside a powered compliant knee exoskeleton. *IEEE Transactions on Neural Systems and Rehabilitation Engineering*, 2014. **22**(6): p. 1128-1137.
- Jamwal, P.K., S. Hussain, and S.Q. Xie, Three-Stage Design Analysis and Multicriteria Optimization of a Parallel Ankle Rehabilitation Robot Using Genetic Algorithm. *IEEE Transactions On Automation Science And Engineering*, 2015. **12**: p. 1433-1446.
- Riener, R., et al., Patient-cooperative strategies for robot-aided treadmill training: First experimental results. *IEEE Transactions on Neural Systems and Rehabilitation Engineering*, 2005. **13**(3): p. 380-394.
- Van Asseldonk, E.H.F., et al., The effects on kinematics and muscle activity of walking in a robotic gait trainer during zero-force control. *IEEE Transactions on Neural Systems and Rehabilitation Engineering*, 2008. **16**(4): p. 360-370.

19. Buerger, S.P. and N. Hogan, Complementary stability and loop shaping for improved human-robot interaction. *IEEE Transactions on Robotics*, 2007. **23**(2): p. 232-244.
20. Miyaguchi, S., et al. Impedance control of pro-/supination based on the skeleton model of upper limbs. in *ICCAS 2007 - International Conference on Control, Automation and Systems*. 2007.
21. Blaya, J.A. and H. Herr, Adaptive Control of a Variable-Impedance Ankle-Foot Orthosis to Assist Drop-Foot Gait. *IEEE Transactions on Neural Systems and Rehabilitation Engineering*, 2004. **12**(1): p. 24-31.
22. Hong, S., et al., Real-time walking pattern generation method for humanoid robots by combining feedback and feedforward controller. *IEEE Transactions on Industrial Electronics*, 2014. **61**(1): p. 355-364.
23. Yuan, J., F. Sun, and Y. Huang, Trajectory Generation and Tracking Control for Double-Steering Tractor-Trailer Mobile Robots With On-Axle Hitching. *IEEE Transactions on Industrial Electronics*, 2015. **62**(12): p. 7665-7677.
24. Alexander Duschau Wicke, J.v.Z., Andrea Caprez, Lars Lunenburger, Robert Riener, Path Control: A Method for Patient-Cooperative Robot Aided Gait Rehabilitation *IEEE Transactions on Neural Systems And Rehabilitation Engineering*, 2010. **18**(1): p. 38-48.
25. Koopman, B., E.H.F. van Asseldonk, and H. Van der Kooij, Speed-dependent reference joint trajectory generation for robotic gait support. *Journal of Biomechanics*, 2014. **47**(6): p. 1447-1458.
26. Martin, P. and M.R. Emami, A neuro-fuzzy approach to real-time trajectory generation for robotic rehabilitation. *Robotics and Autonomous Systems*, 2014. **62**(4): p. 568-578.
27. Jezernik, S., G. Colombo, and M. Morari, Automatic gait-pattern adaptation algorithms for rehabilitation with a 4-DOF robotic orthosis. *IEEE Transactions on Robotics and Automation*, 2004. **20**(3): p. 574-582.
28. Emken, J.L., et al., Feasibility of manual teach-and-replay and continuous impedance shaping for robotic locomotor training following spinal cord injury. *IEEE Transactions on Biomedical Engineering*, 2008. **55**(1): p. 322-334.
29. Martin, P. and M.R. Emami, Real-time fuzzy trajectory generation for robotic rehabilitation therapy. in *2009 IEEE International Conference on Rehabilitation Robotics, ICORR 2009*. 2009.
30. Vallery, H., et al., Reference trajectory generation for rehabilitation robots: Complementary limb motion estimation. *IEEE Transactions on Neural Systems and Rehabilitation Engineering*, 2009. **17**(1): p. 23-30.
31. Sartori, M., D. Farina, and D.G. Lloyd, Hybrid neuromusculoskeletal modeling to best track joint moments using a balance between muscle excitations derived from electromyograms and optimization. *Journal of Biomechanics*, 2014. **47**(15): p. 3613-3621.
32. Hong, J., et al., Gaussian Process Trajectory Learning and Synthesis of Individualized Gait Motions. *IEEE Transactions on Neural Systems and Rehabilitation Engineering*, 2019. **27**(6): p. 1236-1245.
33. Durandau, G., et al., Voluntary control of wearable robotic exoskeletons by patients with paresis via neuromechanical modeling. *Journal of NeuroEngineering and Rehabilitation*, 2019. **16**(1).
34. Ao, D., R. Song, and J. Gao, Movement Performance of Human-Robot Cooperation Control Based on EMG-Driven Hill-Type and Proportional Models for an Ankle Power-Assist Exoskeleton Robot. *IEEE Transactions on Neural Systems and Rehabilitation Engineering*, 2017. **25**(8): p. 1125-1134.
35. Tiboni, M., et al., Robotics rehabilitation of the elbow based on surface electromyography signals. *Advances in Mechanical Engineering*, 2018. **10**(2).
36. Cerone, G.L., A. Botter, and M. Gazzoni, A modular, smart, and wearable system for high density sEMG detection. *IEEE Transactions on Neural Systems and Rehabilitation Engineering*, 2019. **66**(22): p. 3371-3380.
37. Hogan, N., Impedance control: An approach to manipulation: Part II-implementation. *Journal of Dynamic Systems, Measurement and Control, Transactions of the ASME*, 1985. **107**(1): p. 8-16.
38. de Gea, J. and F. Kirchner, Modelling and Simulation of Robot Arm Interaction Forces Using Impedance Control. *IFAC Proceedings Volumes*, 2008. **41**(2): p. 15589-15594.
39. Jamwal, P.K., et al., Musculoskeletal modelling of human ankle complex: Estimation of ankle joint moments. *Clinical Biomechanics*, 2017. **44**: p. 75-82.
40. Safran, M.R., et al., Lateral ankle sprains: A comprehensive review part 2: Treatment and rehabilitation with an emphasis on the athlete. *Medicine and Science in Sports and Exercise*, 1999. **31**(7 SUPPL.): p. S438-S447.
41. Jamwal, P.K., et al., Forward kinematics modelling of a parallel ankle rehabilitation robot using modified fuzzy inference. *Mechanism and Machine Theory*, 2010. **45**(11): p. 1537-1554.
42. Liacouras, P.C. and J.S. Wayne, Computational modeling to predict mechanical function of joints: Application to the lower leg with simulation of two cadaver studies. *Journal of Biomechanical Engineering*, 2007. **129**(6): p. 811-817.
43. Wright, I.C., et al., The effects of ankle compliance and flexibility on ankle sprains. *Medicine and Science in Sports and Exercise*, 2000. **32**(2): p. 260-265.
44. Qian, Z., et al., A dynamic finite element analysis of human foot complex in the sagittal plane during level walking. *PLoS ONE*, 2013. **8**(11).
45. Giddings, V.L., et al., Calcaneal loading during walking and running. *Medicine and Science in Sports and Exercise*, 2000. **32**(3): p. 627-634.
46. Haraguchi, N., et al., Prediction of three-dimensional contact stress and ligament tension in the ankle during stance determined from computational modeling. *Foot and Ankle International*, 2009. **30**(2): p. 177-185.
47. Winters, J.M., Hill-based muscle models: A system engineering perspective, in *Multiple Muscle Systems: Biomechanics and Movement Organization*, J.M. Winters and S.L.-Y. Woo, Editors. 1990, Springer-Verlag: New York. p. 69-91.
48. Wright, I.C., et al., The influence of foot positioning on ankle sprains. *Journal of Biomechanics*, 2000. **33**: p. 513-519.
49. Wright, I.C., et al., The effects of ankle compliance and flexibility on ankle sprains. *Medicine & Science in Sports & Exercise*, 2000. **32**(3): p. 260-265.
50. Yamada, H. and J. Kajzer, A mathematical model of skeletal muscle and numerical simulations of its response under stretching. *JSME International Journal, Series C: Mechanical Systems, Machine Elements and Manufacturing*, 1999. **42**(3): p. 508-513.
51. Fenfang, Z., et al. A computational biomechanical model of the human ankle for development of an ankle rehabilitation robot. in *MESA 2014 - 10th IEEE/ASME International Conference on Mechatronic and Embedded Systems and Applications, Conference Proceedings*. 2014.
52. Myers, B.S., J.H. McElhaney, and B.J. Doherty, The viscoelastic responses of the human cervical spine in torsion: Experimental limitations of quasi-linear theory, and a method for reducing these effects. *Journal of Biomechanics*, 1991. **24**(9): p. 811-817.
53. Funk, J.R., et al., Linear and quasi-linear viscoelastic characterization of ankle ligaments. *Journal of Biomechanical Engineering*, 2000. **122**(1): p. 15-22.
54. Awa, Y. and K. Kobayashi. Kinematics simulation by using ODE and MATLAB. in *Proceedings of the SICE Annual Conference*. 2007.
55. Delp, S.L., et al., OpenSim: Open-Source Software to Create and Analyze Dynamic Simulations of Movement. *Biomedical Engineering, IEEE Transactions on*, 2007. **54**(11): p. 1940-1950.
56. Virtual Animation of the Kinematics of the Human for Industrial Educational and Research purposes (VAKHUM). VAKHUM public dataset. July 14; Available from: [http://www.ulb.ac.be/project/vakhum/public\\_dataset/public\\_data.htm](http://www.ulb.ac.be/project/vakhum/public_dataset/public_data.htm).
57. Krebs, H.I., et al., Rehabilitation robotics: Performance-based progressive robot-assisted therapy. *Autonomous Robots*, 2003. **15**(1): p. 7-20.
58. Tsoi, Y.H. and S.Q. Xie. Impedance control of ankle rehabilitation robot. in *2008 IEEE International Conference on Robotics and Biomimetics, ROBIO 2008*. 2008.
59. Derrac, J., et al., A practical tutorial on the use of nonparametric statistical tests as a methodology for comparing evolutionary and swarm intelligence algorithms. *Swarm and Evolutionary Computation*, 2011. **1**(1): p. 3-18.